The Astrophysical Journal, 729:103 (14pp), 2011 March 10 doi:10.1088/0004-637X/729/2/103

UNRAVELING THE NATURE OF UNIDENTIFIED HIGH GALACTIC LATITUDE *FERMI*/LAT GAMMA-RAY SOURCES WITH *SUZAKU*

K. Maeda[1], J. Kataoka[1], T. Nakamori[1], Ł. Stawarz[2,3], R. Makiya[4], T. Totani[4], C. C. Cheung[5], D. Donato[6,7], N. Gehrels[7], P. Saz Parkinson[8], Y. Kanai[9], N. Kawai[9], Y. Tanaka[2], R. Sato[2], T. Takahashi[2], and Y. Takahashi[1]
[1] Research Institute for Science and Engineering, Waseda University, 3-4-1 Okubo, Shinjuku, Tokyo 169-8555, Japan; ko-t.maeda.x-6@ruri.waseda.jp
[2] Institute of Space and Astronautical Science (ISAS), Japan Aerospace Exploration Agency (JAXA), 3-1-1 Yoshinodai, Chuo-ku, Sagamihara, Kanagawa 252-5510, Japan
[3] Astronomical Observatory, Jagiellonian University, ul. Orla 171, Kraków 30-244, Poland
[4] Department of Astronomy, Kyoto University, Kitashirakawa, Sakyo-ku, Kyoto 606-8502, Japan
[5] NRC Research Associate, Space Science Division, Naval Research Laboratory, Washington, DC 20375, USA
[6] Center for Research and Exploration in Space Science and Technology (CRESST) and NASA Goddard Space Flight Center, Greenbelt, MD 20771, USA
[7] NASA Goddard Space Flight Center, Greenbelt, MD 20771, USA
[8] Santa Cruz Institute for Particle Physics (SCIPP), University of California, Santa Cruz, Natural Sciences II, Room 313, 1156 High Street, Santa Cruz, CA 95064, USA
[9] Department of Physics, Tokyo Institute of Technology, 2-12-1 Ohokayama, Meguro, Tokyo 152-8551, Japan
Received 2010 August 28; accepted 2011 January 10; published 2011 February 15

ABSTRACT

Here we report on the results of deep X-ray follow-up observations of four unidentified γ-ray sources detected by the *Fermi*/LAT instrument at high Galactic latitudes using the X-ray Imaging Spectrometers on board the *Suzaku* satellite. All of the studied objects were detected with high significance during the first three months of *Fermi*/LAT operation and subsequently better localized in the first *Fermi*/LAT catalog (1FGL). For some of them, possible associations with pulsars and active galaxies have subsequently been discussed, and our observations provide an important contribution to this debate. In particular, a bright X-ray point source has been found within the 95% confidence error circle of 1FGL J1231.1−1410. The X-ray spectrum of the discovered *Suzaku* counterpart of 1FGL J1231.1−1410 is well fitted by a blackbody with an additional power-law component. This supports the recently claimed identification of this source with a millisecond pulsar PSR J1231−1411. For the remaining three *Fermi* objects, on the other hand, the X-ray observations performed are less conclusive. In the case of 1FGL J1311.7−3429, two bright X-ray point sources were found within the LAT 95% error circle. Even though the X-ray spectral and variability properties for these sources were robustly assessed, their physical nature and relationship with the γ-ray source remain uncertain. Similarly, we found several weak X-ray sources in the field of 1FGL J1333.2+5056, one coinciding with the high-redshift blazar CLASS J1333+5057. We argue that the available data are consistent with the physical association between these two objects, although the large positional uncertainty of the γ-ray source hinders a robust identification. Finally, we have detected an X-ray point source in the vicinity of 1FGL J2017.3+0603. This *Fermi* object was recently suggested to be associated with a newly discovered millisecond radio pulsar PSR J2017+0603, because of the spatial coincidence and the detection of the γ-ray pulsations in the light curve of 1FGL J2017.3+0603. Interestingly, we have detected the X-ray counterpart of the high-redshift blazar CLASS J2017+0603, located within the error circle of the γ-ray source, while we were only able to determine an X-ray flux upper limit at the pulsar position. All in all, our studies indicate that while a significant fraction of unidentified high Galactic latitude γ-ray sources is related to the pulsar and blazar phenomena, associations with other classes of astrophysical objects are still valid options.

Key words: galaxies: active – gamma rays: general – pulsars: general – radiation mechanisms: non-thermal – X-rays: general

1. INTRODUCTION

Observations with the EGRET instrument on board the *Compton Gamma-Ray Observatory* (*CGRO*) in the 1990s opened a new window in studying MeV–GeV emissions from both Galactic and extragalactic objects. Despite over a decade of multi-wavelength follow-up studies, more than 60% of the γ-ray emitters included in the third EGRET catalog (3EG; Hartman et al. 1999) are yet to be identified (that is, 170 out of 271). This is mainly because of the relatively poor γ-ray localizations of EGRET sources (typical 95% confidence radii, $r_{95} \simeq 0.^{\circ}4$–$0.^{\circ}7$), making the identification procedure challenging especially for the objects located within the Galactic plane, due to source confusion. In particular, as much as $\simeq$90% of the 3EG sources detected at Galactic latitudes $|b| < 10^{\circ}$ do not have robustly selected counterparts at lower frequencies. On the other hand, most of the 3EG sources at high Galactic latitudes have been associated with blazars—a subclass of jetted active galactic nuclei (AGNs) displaying strong relativistic beaming—in accordance with the expectation for the extragalactic population to dominate the γ-ray sky at $|b| > 10^{\circ}$ (Abdo et al. 2009a). Yet the unidentified fraction of the high Galactic latitude 3EG sources is still large ($\simeq$30%; e.g., Sowards-Emmerd et al. 2003). The situation is basically unchanged in the revised EGRET catalog (EGR; Casandjian & Grenier 2008), even though the revised background modeling applied in the EGR resulted in fewer γ-ray detections (188 sources in total, in contrast to 271 listed in 3EG); 87 out of 188 EGR entries remain unidentified.

The unidentified low Galactic latitude γ-ray sources are expected to be associated with local objects such as molecular clouds, supernova remnants, massive stars, pulsars and pulsar wind nebulae, or X-ray binaries (see, e.g., Gehrels & Michelson

1999 and references therein). Meanwhile, the population of unidentified high Galactic latitude γ-ray sources is typically believed to be predominantly extragalactic in origin, although there is a suspected Galactic component as well (Özel & Thompson 1996). For example, the brightest steady source 3EG J1835+5918 located at $|b| > 10^{\circ}$ was proposed to be associated with an isolated neutron star (Mirabal et al. 2000; Reimer et al. 2001). The neutron star origin and its association with the γ-ray source have been confirmed with the discovery of a γ-ray pulsar at the position of 3EG J1835+5918 with *Fermi*/LAT (Abdo et al. 2010a, 2010b). Similarly, high-energy γ-ray pulsations from PSR J2021+3651, which was long considered as a likely pulsar counterpart of 3EG J2021+3716 (Halpern et al. 2008), were discovered with *Fermi* (Abdo et al. 2009b) and *AGILE* (Tavani et al. 2009). On the other hand, blazar G74.87+1.22 (B 2013+370) was claimed to be the most likely counterpart of the unidentified object 3EG J2016+3657 located within the Galactic plane (Mukherjee et al. 2000; Halpern et al. 2001). Other unidentified γ-ray sources were similarly investigated with varying success (e.g., Mukherjee & Halpern 2004). We note that population studies, which could in principle shed some light on the galactic/extragalactic origin of different classes of unidentified EGRET sources, were impeded by different levels of background emission at different locations from the Galactic plane and different EGRET exposure for various parts of the sky (see the discussion in Reimer 2001). Also, variability studies were previously hampered by the limited statistics and noncontinuous EGRET observations (Nolan et al. 2003).

With the successful launch of the *Fermi* Gamma-ray Space Telescope, we now have a new opportunity to study γ-ray emission from different types of high-energy sources with much improved sensitivity and localization capabilities than with EGRET. With its field of view (five times larger than that of EGRET) covering 20% of the sky at every moment, and its improved sensitivity (by more than an order of magnitude with respect to EGRET), the Large Area Telescope (LAT; Atwood et al. 2009) aboard *Fermi* surveys the entire sky each day down to a photon flux level of $F_{>100\,\mathrm{MeV}} \simeq$ few $\times$ 10^{-7} photons cm^{-2} s^{-1}. The first *Fermi*/LAT point-source catalog (1FGL) already surpasses EGRET with 1451 sources detected at significance levels $>4\sigma$ within the 100 MeV–100 GeV photon energy range during the initial 11 month survey (Abdo et al. 2010c). Several high-latitude EGRET sources lacking low-frequency counterparts were confirmed by *Fermi*/LAT and associated with previously unknown γ-ray blazars, as expected (Abdo et al. 2010d). Somewhat surprisingly, however, a number of γ-ray emitters at $|b| > 10^{\circ}$ have been robustly identified by LAT with newly found γ-ray pulsars via the detection of γ-ray pulsations (Abdo et al. 2010e). Most of these are in fact millisecond pulsars (MSPs). A diminishing, yet still significant, population of unidentified *Fermi*/LAT objects remains, constituting as much as about 40% of all 1FGL sources. This includes more than 10 unidentified EGRET sources at high Galactic latitudes, which are thus the best candidates for the persistent, or even "steady" γ-ray emitters over the 10-year-long period between the EGRET and *Fermi*/LAT epochs (as indicated by their comparable photon fluxes in the 3EG and 1FGL catalogs).

Thus motivated, we started a new project to investigate the nature of unidentified high Galactic latitude *Fermi* objects through deep X-ray follow-up observations with the Japanese X-ray astronomy satellite *Suzaku* (Mitsuda et al. 2007). This paper presents the results of the first year campaign conducted over the span of *Suzaku*-AO4 (2009 April–2010 March), during which we have observed four steady/weakly variable *Fermi*/LAT sources from the three-month *Fermi*/LAT Bright Source List (0FGL; Abdo et al. 2009c). These are denoted below according to their 1FGL catalog entries as 1FGL J1231.1−1410, 1FGL J1311.7−3429, 1FGL J1333.2+5056, and 1FGL J2017.3+0603. Thanks to the superb localization provided by the LAT, all the corresponding 95% error circles (typically $r_{95} \simeq 0.^{\circ}1$–$0.^{\circ}2$) could be covered within the field of view of the *Suzaku* X-ray CCD camera "XIS." Only in the case of 1FGL J1333.2+5056, the *Suzaku* pointing does not cover the entire 95% LAT error circle since the localization error for this object did not improve sufficiently between 1FGL and 0FGL. Along with our *Suzaku* observations, systematic pulsar searches with radio telescopes have been performed for the *Fermi*/LAT unassociated sources. These resulted in new discoveries of MSPs co-located with the two γ-ray sources included in our study (1FGL J1231.1−1410 and 1FGL J2017.3+0603). In both cases, *Fermi*/LAT eventually detected γ-ray pulsations as well, in accordance with the results in the radio domain (Ransom et al. 2010; Cognard et al. 2011). Our deep X-ray exposure discussed in the next sections supports the pulsar identification for at least 1FGL 1231.1−1410, but is less conclusive in the case of 1FGL J2017.3+0603. For the other target from our list, 1FGL J1333.2+5056, a tentative association with blazar CLASS J1333+5057 was claimed in the LAT Bright AGN Sample (LBAS; Abdo et al. 2009a). Here we substantiate this possibility by presenting the broadband spectral energy distribution (SED) for 1FGL J1333.2+5056/CLASS J1333+5057, including new *Suzaku* data, which is indeed typical of a flat spectrum radio quasar (FSRQ). Finally, the nature of the remaining source 1FGL J1311.7−3429 (for which no radio or γ-ray pulsations have been detected so far; Ransom et al. 2010) could not be revealed, despite the discovery of a likely X-ray counterpart. In particular, we found that the multi-wavelength spectrum of 1FGL J1311.7−3429 is not consistent with either a typical blazar or pulsar spectrum.

In Section 2, we describe the *Suzaku* X-ray follow-up observations and the data reduction procedure. The results of the analysis are given in Section 3. The discussion and conclusions are presented in Sections 4 and 5, respectively. A standard ΛCDM cosmology with $\Omega_{\Lambda} = 0.73$, $\Omega_{\mathrm{M}} = 0.27$, and $H_0 = 71$ km s^{-1} Mpc^{-1} is assumed throughout the paper.

2. OBSERVATIONS AND ANALYSIS

2.1. Observations and Data Reduction

We observed four unidentified high Galactic latitude *Fermi*/LAT objects with the *Suzaku* X-ray astronomy satellite (Mitsuda et al. 2007). These are denoted in the 1FGL catalog as 1FGL J1231.1−1410, 1FGL J1311.7−3429, 1FGL J1333.2+5056, and 1FGL J2017.3+0603 (see Abdo et al. 2010c). All the sources but one (1FGL J2017.3+0603) were already listed in the 3EG (Hartman et al. 1999) and their γ-ray fluxes are given in Table 1. The *Suzaku* observation logs are summarized in Table 2. The observations were made with three out of four CCD cameras (X-ray Imaging Spectrometers, XIS; Koyama et al. 2007) and a Hard X-ray Detector (HXD; Kokubun et al. 2007; Takahashi et al. 2007). One of the XIS sensors is a back-illuminated CCD (BI; XIS1), and the other three XIS sensors are front-illuminated ones (FI; XIS0, XIS2, and XIS3; the operation of XIS2 has been terminated in 2006 November).

Table 1
EGRET and *Fermi*/LAT Entries for the Analyzed Objects

Name	R.A. (deg)	Decl. (deg)	l (deg)	b (deg)	$F_{0.1-20\,\mathrm{GeV}}$ (10^{-8} photons cm^{-2} s^{-1})	$r_{95\%}$ (deg)
1FGL J1231.1−1410[a]	187.80	−14.17	295.53	+48.41	14.9 ± 0.7	0.03
3EG J1234−1318	188.19	−16.30	296.43	+49.34	21.6 ± 5.3	0.76
(EGR J1231−1412)						
1FGL J1311.7−3429[b]	197.95	−34.49	307.69	+28.19	11.7 ± 1.1	0.04
3EG J1314−3431	198.51	−34.52	308.21	+28.12	18.7 ± 3.1	0.56
(EGR J1314−3417)						
1FGL J1333.2+5056[b]	203.30	+50.94	107.32	+64.90	4.5 ± 1.0	0.15
3EG J1337+5029	204.39	+50.49	105.40	+65.04	9.2 ± 2.6	0.72
(EGR J1338+5102)						
1FGL J2017.3+0603[c]	304.34	+6.05	48.62	−16.02	4.5 ± 0.5	0.04

Notes.
[a] Data consistent with no variability between EGRET and *Fermi*/LAT observations.
[b] The γ-ray fluxes determined by EGRET and *Fermi*/LAT marginally consistent within the 2σ level.
[c] Data consistent with no variability between EGRET and *Fermi*/LAT observations because the EGRET detection limit $\simeq 6 \times 10^{-8}$ photons cm^{-2} s^{-1}.

Table 2
Suzaku/XIS Observation Log

Name	ObsID	Pointing Center[a]		Observation Start	Effective Exposure
		R.A. (deg)	Decl. (deg)	(UT)	(ks)
1FGL J1231.1−1410	804017010[b]	187.8001	−14.1665	2009 Jul 8 22:53:48	23.8
	804017020[b]	187.7993	−14.1672	2009 Jul 28 05:21:37	44.8
1FGL J1311.7−3429	804018010	197.9603	−34.4918	2009 Aug 4 04:56:35	33.0
1FGL J1333.2+5056	804019010	203.2955	51.0170	2009 Jun 1 10:13:15	39.1
1FGL J2017.3+0603	804020010	304.3461	6.0496	2009 Oct 27 10:14:45	26.7

Notes.
[a] The pointing centers were the positions given in the 0FGL catalog (Abdo et al. 2009c).
[b] The requested continuous 80 ks *Suzaku* exposure was interrupted by the Target of Opportunity (ToO) observation of GRB 090708. For this reason, the observation was divided into 30 ks and 50 ks segments before and after the ToO observation.

Since none of the studied sources have been detected with the HXD, in this paper we focus on the analysis of only the XIS data. The XIS was operated in the pointing source mode and in the normal clocking mode during all the exposures.

In the reduction and the analysis of the *Suzaku* data, HEADAS software version 6.7 and a calibration database (CALDB; released on 2009 September 25) were used. The XIS cleaned event data set was obtained in the combined 3×3 and 5×5 edit modes using `xselect`. We excluded the data collected during the time and up to 60 s after *Suzaku* was passing the South Atlantic Anomaly (SAA). We also excluded the data corresponding to less than 5° of the angle between Earth's limb and the pointing direction (the elevation angle, ELV). Moreover, we excluded time windows during which the spacecraft was passing through the low cut-off rigidity (COR) of below 6 GV. Finally, we removed hot and flickering pixels (using `sisclean`; Day et al. 1998). With all the aforementioned data selection criteria applied, the resulting total effective exposures for all the observed sources are summarized in Table 2.

2.2. Analysis

XIS images for each target were extracted from the two FI CCDs (XIS0, XIS3) within the photon energy range from 0.4 to 10 keV. In the image analysis procedure, calibration sources located at the corners of CCD chips were excluded. The images of non-X-ray background (NXB) were obtained from the night Earth data using `xisnxbgen` (Tawa et al. 2008). Since the exposure times for the original data were different from that of NXB, we calculated the appropriate exposure-corrected original and NXB maps using `xisexpmapgen` (Ishisaki et al. 2007). The corrected NXB images were next subtracted from the corrected original images. In addition, we simulated flat sky images using `xissim` (Ishisaki et al. 2007) and applied a vignetting correction. All the images obtained with XIS0 and XIS3 were combined and re-binned by a factor of four. All the FI XIS images were in addition smoothed by a Gaussian function with $\sigma = 0.'17$, and the resultant images are presented in Section 3. Note that the apparent features at the edge of these exposure-corrected images are undoubtedly spurious due to low exposure in those regions. For further analysis, source regions were carefully selected around each detected X-ray sources within the error circle of a studied γ-ray emitter. The corresponding background regions with radius $3'$ were taken from the same XIS chips avoiding any bright X-ray spots in the field. In all the cases, such source regions were set to within $3'$ or $1'$ radii around the X-ray point sources (because of the blurring due to the *Suzaku*/XIS point-spread function, PSF), depending on the properties of each analyzed field. The source detection criterion was based on a signal-to-noise ratio which is defined, assuming a Poisson distribution, as the ratio of the excess events above a background to its standard deviation. Photon counts were derived from each source and background regions and we set the detection threshold at 4σ. The source positions and the

Table 3
Source Detection Results of the *Suzaku* Observation

Name	Source ID	Position		Detection Significance	$r_{95\%}$
		R.A. (deg)	Decl. (deg)	σ	(arcsec)
1FGL J1231.4−1410	···	187.790	−14.192	13.67	7.44
1FGL J1311.7−3429	src A	197.939	−34.508	15.52	17.44
	src B	197.942	−34.534	12.89	12.27
1FGL J1333.2+5056	src A	203.252	50.983	8.53	23.34
	src B	203.161	51.032	7.27	19.97
	src C	203.276	51.014	7.47	20.75
	src D	203.479	50.967	4.50	38.41
	src E	203.381	50.892	4.91	26.51
1FGL J2017.3+0603	···	304.310	6.052	14.44	4.73

corresponding errors were obtained by fitting a two-dimensional Gaussian around each X-ray spot. The source detection results are summarized in Table 3.

The light curves were constructed for each potential X-ray counterpart of the observed *Fermi* objects. Each light curve provides net-counting rates, with the count rates of the corresponding background region subtracted. In the timing analysis, the FI (XIS0, XIS3) and BI (XIS1) CCD's light curves were combined using `lcmath` and then re-binned using `lcurve`. To assess statistical significances of the flux variations, the χ^2 test was applied to each constructed data set (probing a constant flux hypothesis with `lcstats` command). Finally, the XIS spectra for each source region were extracted, with the same corresponding background spectra as defined in the image analysis (see above). RMF files for the detector response and ARF files for the effective area were generated using `xisrmfgen` and `xissimarfgen` (Ishisaki et al. 2007). In this spectral analysis, all the selected data from the FI CCDs were co-added (using `mathpha`) without calculating Poisson errors, and the response files were combined with the `marfrmf` and `addrmf` commands. Since all the studied *Fermi*/LAT objects are located at high Galactic latitudes, the absorption of soft X-ray photons was set to the Galactic one with the equivalent column density of a neutral hydrogen, $N_{\rm H}$, as given in Dickey & Lockman (1990). In some cases where apparent systematic features are visible as trends of the residuals with energy (see Figure 3), we attempted to use an inter-calibration constant between the FI and BI CCDs to improve the fits. From this inspection, we found negligible improvement of the fits; thus, we conclude that the limited photon statistics is predominantly responsible for the somewhat unsatisfactory model fits to the data.

3. RESULTS

3.1. 1FGL J1231.4−1410

Our *Suzaku* observations (interrupted for ≃20 days[10]) revealed one X-ray point source (R.A., decl.)= (187.°790(1), −14.°192(1)) within the LAT error circle of 1FGL J1231.4−1410. Figure 1 shows the corresponding X-ray image, prepared as described in Section 2.2. For further analysis, the source extraction region was set to within a 3′ radius around the X-ray intensity peak, and the corresponding background region was chosen as indicated in Figure 1. The light curve of the X-ray source with a time bin of 900 s is presented in Figure 2. The upper panel shows the count rate variation during the first observation, while the bottom panel shows that of the second observation. The light curves of the two periods can both be well fitted by a constant count rate of 3.03×10^{-2} counts s^{-1}, with $\chi^2/{\rm dof} = 58.3/107$. This indicates that the X-ray emission of the analyzed source is steady, with the χ^2 probability for a constant flux >99%.

The X-ray spectrum of the *Suzaku* source, which we propose to be the most likely counterpart of 1FGL J1231.1−1410, is shown in Figure 3. The energy range used for the fitting was set as 0.4–7.0 keV. First, we fit the X-ray spectrum by a blackbody emission moderated by the Galactic absorption only (Morrison & McCammon 1983). This fit was not acceptable, however, due to significant residuals above 2 keV ($\chi^2/{\rm dof} = 128.1/34$; see Figure 3, left panel, where the excess emission above 2 keV has been enhanced by fixing the blackbody parameters to those determined by the data below 2 keV only). The situation was essentially unchanged when the column density was treated as a free parameter. In this case, the residuals above 2 keV remained, but the returned value of $N_{\rm H}$ was then consistent with zero. To account for the >2 keV emission, we therefore added a power-law component to the thermal one and fixed $N_{\rm H} = 0$. The goodness of the fit was in this way substantially improved to χ^2 of 55.46/32, supporting the presence of a non-thermal tail in the spectrum of the analyzed object (see Figure 3). In order to further confirm the reality of this finding, we analyzed the highest quality FI CCD (XIS0, XIS3) data which had sufficient photon statistics within the 2–8 keV range, examining various approaches for the background estimation, namely (1) the background taken from the same CCD chips but off-axis, as given in Figure 1, (2) the concentric ring background surrounding the source region on the same CCD chips, and (3) the background for the same region as the source estimated from the Lockman Hole observation taken with the same XIS mode at nearby dates (ObsID = 104002010). In all of the examined approaches, the presence of the non-thermal component in the X-ray spectrum of 1FGL J1231.1−1410 could be confirmed at high significance, as summarized in Tables 4 and 5.

To sum up, we conclude that the X-ray counterpart of 1FGL J1231.1−1410 is robustly characterized by a blackbody-type spectrum with a temperature of $kT \simeq 0.16 \pm 0.03$ keV plus a power-law tail with the photon index of $\Gamma \simeq 1.79^{+0.40}_{-0.17}$. The energy flux of the non-thermal component is $S_{2-8\,{\rm keV}} \simeq 5.81 \times 10^{-14}$ erg cm^{-2} s^{-1}, which can be compared with the *Fermi*/LAT energy flux $S_{0.1-10\,{\rm GeV}} \simeq (1.06 \pm 0.06) \times 10^{-10}$ erg cm^{-2} s^{-1}, as given in the 1FGL catalog. Thus, the extrapolation of the X-ray power-law component to the γ-ray range yielding the 0.1–10 GeV energy flux ≃5.74×10^{-13} erg cm^{-2} s^{-1} falls orders of magnitudes below the observed one. This

[10] The exposure was interrupted because of the Target of Opportunity observation of GRB 090708.

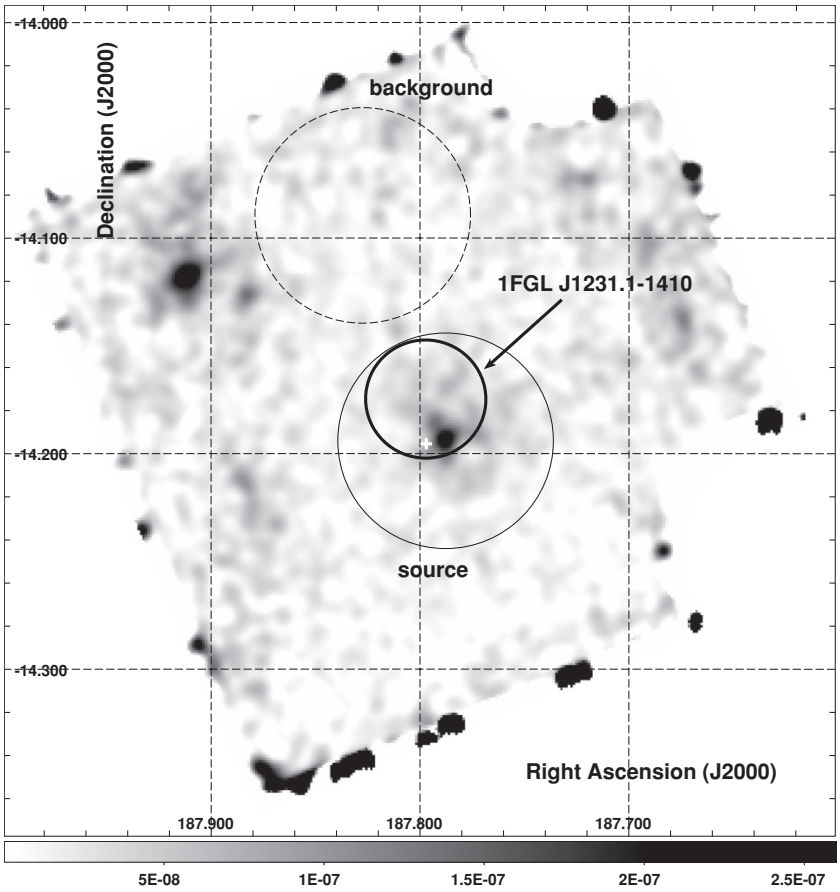

Figure 1. *Suzaku*/XIS FI (XIS0+3) image of the 1FGL J1231.1−1410 region in the 0.4–10 keV photon energy range. The image shows the relative excess of smoothed photon counts (arbitrary units indicated in the bottom bar) and is displayed with linear scaling. The areas enclosed by the solid and dashed circles are the source and background regions, respectively. The thick solid circle denotes the 95% position error of 1FGL J1231.1−1410. The white cross marks the position of the radio MSP, PSR J1231−1411 (Ransom et al. 2010).

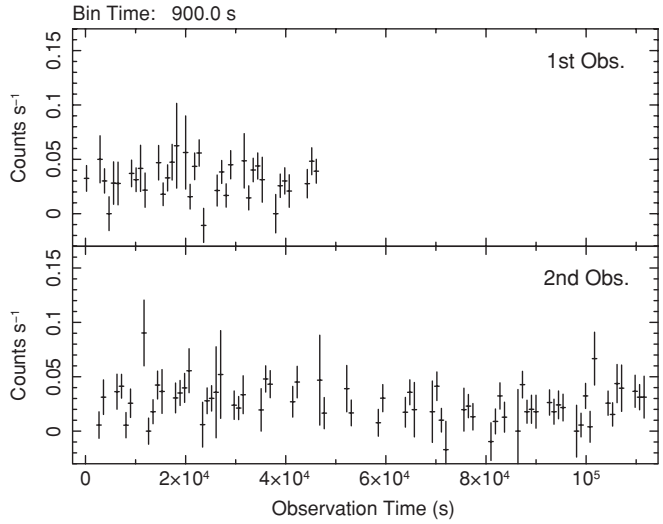

Figure 2. *Suzaku*/XIS light curves of the X-ray counterpart of 1FGL J1231.1−1410 during the first and second observations (upper and lower panels, respectively). Binning time applied is 900 s. The zero points of the upper and lower panels are MJD 55020.9971 and 55040.2343, respectively (TDB: Barycentric Dynamical Time).

implies either a multi-component character or a concave spectral form of the high-energy X-ray-to-γ-ray continuum of 1FGL J1231.1−1410, and both possibilities should be kept in mind in the context of a very likely association of the discussed source with an MSP. Indeed, the MSP PSR J1231−1411 (marked by a white cross in Figure 1) was recently found by Ransom et al. (2010) via the detection of radio pulsations with the pulse period of 3.68 ms within the LAT error circle of 1FGL J1231.1−1410 using the Green Bank Telescope (GBT), just after our *Suzaku* observations. In addition, the *Fermi* spectrum shows a cutoff at around a few GeV, which is consistent with the typical spectrum of MSPs (Ransom et al. 2010). The X-ray emitter observed by *Suzaku* is located roughly 40″ away from the newly discovered MSP PSR J1231−1411 (Ransom et al. 2010; see Figure 1), but considering the limited pointing accuracy of the *Suzaku*/XIS ($\lesssim$1′), both objects can be considered as cospatial. In fact, as described in Ransom et al. (2010), a *Swift*/XRT source at (R.A., decl.) = (187.7972,−14.1953) coinciding with the *Suzaku* one was found to be positionally consistent (within the 90% error of 5.″5) with that of the MSP PSR J1231−1411.

3.2. 1FGL J1311.7−3429

Two X-ray point sources were found within the LAT error circle of 1FGL J1311.7−3429. Figure 4 shows the corresponding X-ray image with the northern *Suzaku* object, src A, located at (R.A., decl.) = (197.°939(1), −34.°508(2)) and the southern source, src B, positioned at (R.A., decl.) = (197.°942(1), −34.°534(2)). Note that src B is situated just marginally within the edge of the *Fermi*/LAT error circle. For further analysis, we

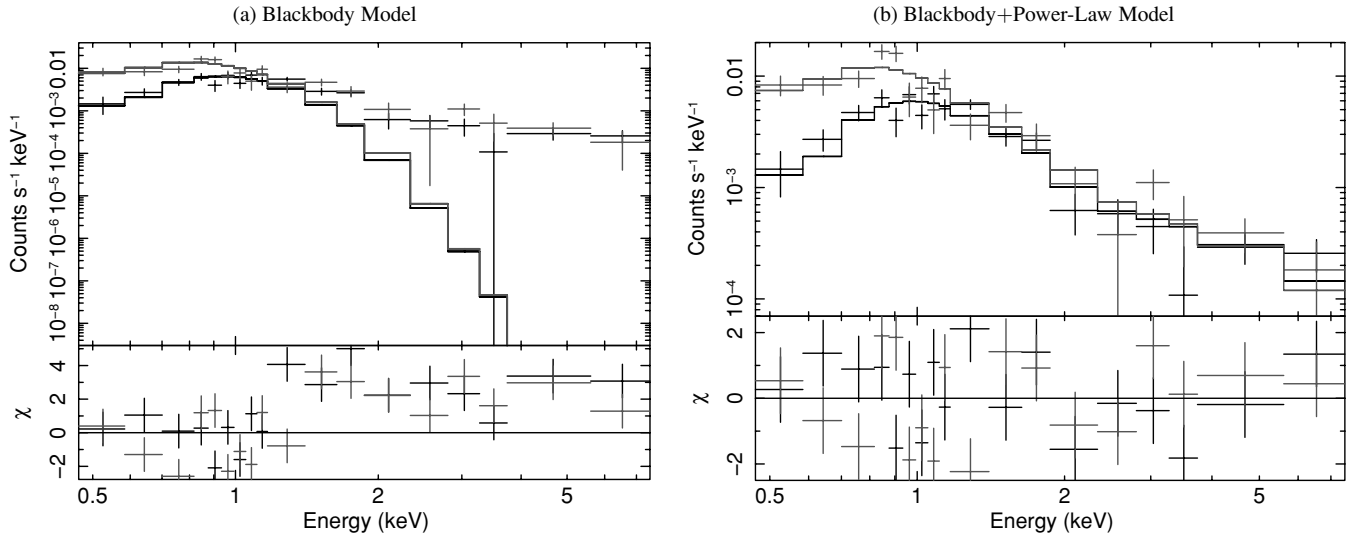

Figure 3. *Suzaku*/XIS spectra of the X-ray counterpart of 1FGL J1231.1−1410 in the photon energy range 0.4–7.0 keV fitted with the blackbody model (a) and blackbody+power-law model (b). FI data are shown in black, and BI data in gray.

Table 4
Fitting Parameters for 1FGL J1231.1−1410 in the Framework of Blackbody (BB) and Power-law (PL) Models

Parameter	BB Model Value and Error	BB+PL Model Value and Error
$N_{\rm H}$ (10^{22} cm^{-2})	0.0 (fixed)	0.0 (fixed)
kT (keV)	0.228 ± 0.008	$0.163^{+0.024}_{-0.026}$
Norm. (BB)	$(1.42 \pm 0.14) \times 10^{-6}$	$(1.20^{+0.31}_{-0.37}) \times 10^{-6}$
Γ	...	$1.79^{+0.40}_{-0.17}$
Norm. (PL)	...	$(1.94^{+1.14}_{-0.84}) \times 10^{-5}$
χ^2	128.1	55.46
dof	34	32
Reduced χ^2	3.768	1.733
Flux (2–8 keV) (erg cm^{-2} s^{-1})	...	$(5.79^{+1.62}_{-1.52}) \times 10^{-14}$

Table 5
Blackbody (BB) and Power-law (PL) Components in the X-ray Spectrum of 1FGL J1231.1−1410

Statistics	(i) Standard Background		(ii) Ring Background		(iii) Lockman Hole Background	
	BB	BB+PL	BB	BB+PL	BB	BB+PL
χ^2	134.71	56.16	67.21	18.97	39.77	23.97
dof	34	32	30	28	38	36
F value	22.4		35.6		11.9	
Probability	8.33×10^{-7}%		2.04×10^{-6}%		1.10×10^{-2}%	

set the source regions to within 1′ radii around the respective X-ray flux maxima. The derived light curves of src A and src B with time bins of 450 s are presented in Figure 5 (upper and lower panels, respectively). As shown, during the first 20 ks of the observation, src A exhibited a very rapid X-ray flare, with the count rate changing by a factor of 10. After the flare, however, the X-ray flux of src A remained steady. A constant fit to the light curve of src A returns χ^2/dof = 403.9/97, and hence the variability of this source is statistically significant. On the other hand, src B was characterized by a constant flux over the duration of the exposure (χ^2/dof = 45.0/97) with a count rate of 1.3×10^{-2} counts s^{-1}.

Figure 6 shows the spectra of src A and src B within the energy range 0.4–8.0 keV. The best model fits for both newly discovered X-ray objects consist of power-law continua with photon indices $\Gamma \simeq 1.38 \pm 0.13$ (src A) and $\Gamma \simeq 1.34 \pm 0.16$ (src B), moderated by the Galactic absorption. Details of the model fitting are summarized in Table 6. Note that the observed X-ray spectra of the two sources are very similar, and the X-ray fluxes of the objects are almost identical. It is important to emphasize at this point that because of the relatively large PSF of *Suzaku*/XIS (a half-power diameter of ∼3′), it is quite difficult to separate completely src A and src B—located only 1.′6 apart—for the purpose of spectral analysis. As a result, even though it is clear that we are dealing with two physically distinct X-ray sources (each detected at high significance), their spectral parameters cannot be accessed robustly.

3.3. 1FGL J1333.2+5056

Our *Suzaku* observations revealed multiple regions of enhanced X-ray emission inside the LAT error circle of 1FGL J1333.2+5056, as shown in the corresponding X-ray image in Figure 7. The associations of these faint X-ray sources with 1FGL J1333.2+5056 are therefore quite ambiguous. Within the *Fermi*/LAT error circle covered by the XIS exposure,[11] five X-ray enhancements have been found with detection significances of more than 4σ, and these are denoted here as src A, B, C, D, and E (see Figure 7 and Table 3).

The light curves of src A, B, C, D, and E with 5760 s binning are shown in Figure 8 in descending order. As noted above, all the analyzed X-ray sources are very dim, with X-ray fluxes at the level of $\sim 10^{-14}$ erg cm^{-2} s^{-1}. Hence, we could not assess the variability properties of the selected objects by means of the χ^2 test with a constant flux hypothesis (see Table 7). The spectra of the five X-ray sources, all extracted within 1′ source radii, are shown in Figure 9. Again, limited photon statistics precluded any detailed analysis, and therefore in the model fitting we

[11] Note that the 1FGL localization error for the analyzed γ-ray object did not improve sufficiently between 0FGL and 1FGL. For this reason, we could not cover the entire 95% LAT error circle of 1FGL J1333.2+5056 within one pointing of *Suzaku*/XIS.

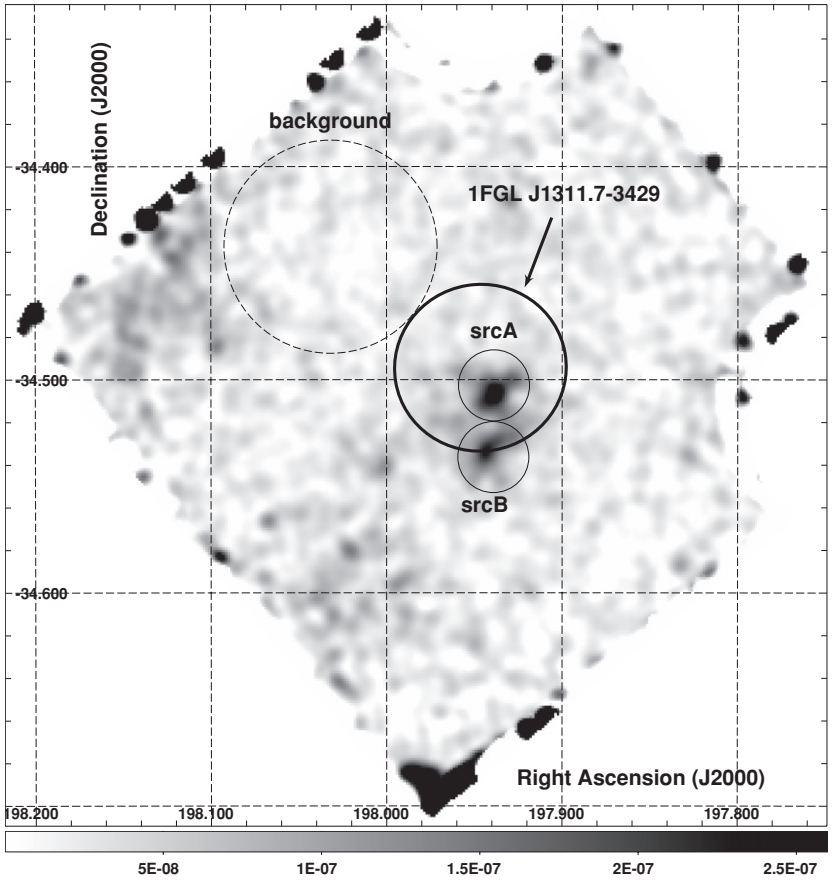

Figure 4. *Suzaku*/XIS FI (XIS0+3) image of the 1FGL J1311.7−3429 region in the 0.4–10 keV photon energy range. The image shows the relative excess of smoothed photon counts (arbitrary units indicated in the bottom bar) and is displayed with linear scaling. The regions enclosed by the solid and dashed circles are the source and background regions, respectively. The thick solid circle denotes the 95% position error of 1FGL J1311.7−3429. Within this error circle, two potential X-ray counterparts of the γ-ray source were found: src A and src B.

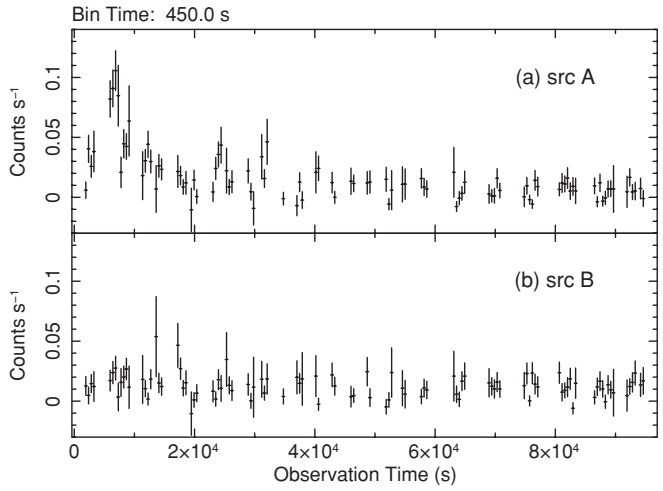

Figure 5. *Suzaku*/XIS light curves of two potential X-ray counterparts of 1FGL J1311.7−3429 with 450 s binning. The northern source src A (upper panel) showed a highly significant X-ray flare in the first 20 ks of observation, during which the count rate increased by a factor of 10. The southern source src B (lower panel) was steady during the whole exposure. The zero point of src A and src B is MJD 55047.2280 (TDB).

applied only single power-law models moderated by the Galactic absorption. The results are summarized in Table 8. We also emphasize that the 1FGL error circle unfortunately runs off the edge of *Suzaku* field of view. For all these reasons, we cannot

Table 6
Fitting Parameters for 1FGL J1311.7−3429 for the Power-law Model

Parameter	src A Value and Error	src B Value and Error
$N_{\rm H}$ (10^{20} cm^{-2})	4.45 (fixed)	4.45 (fixed)
Γ	$1.38^{+0.13}_{-0.13}$	$1.34^{+0.16}_{-0.15}$
Norm.	$(2.69^{+0.38}_{-0.37}) \times 10^{-5}$	$(2.08^{+0.34}_{-0.33}) \times 10^{-5}$
χ^2	42.6	42.1
dof	38	38
Reduced χ^2	1.12	1.11
Flux (2–8 keV) (erg cm^{-2} s^{-1})	$(1.45^{+0.18}_{-0.18}) \times 10^{-13}$	$(1.20^{+0.18}_{-0.17}) \times 10^{-13}$

persuasively identify an X-ray counterpart of the γ-ray source 1FGL J1333.2+5056. Nevertheless, we note that one of the X-ray enhancements, src D, coincides with the $z = 1.362$ FSRQ CLASS J1333+5057 (marked in Figure 7 by a white cross; Shaw et al. 2009), listed in the 1FGL as a possible association with 1FGL J1333.2+5056. Note however the relatively low significance of the detection of this source with *Suzaku*/XIS.

3.4. 1FGL J2017.3+0603

A single prominent X-ray point source was found at the edge of the 1FGL error circle of the unidentified γ-ray source 1FGL J2017.3+0603. The X-ray source is located at (R.A., decl.) = (304.°310(1), 6.°052(1)), as shown in Figure 10. For

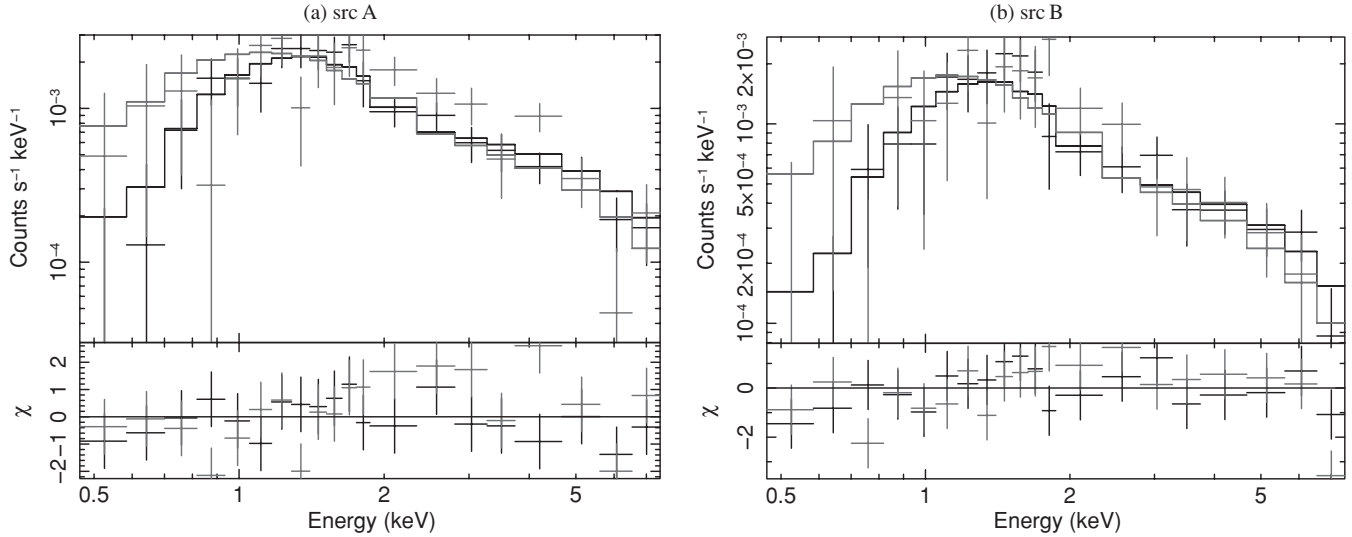

Figure 6. *Suzaku*/XIS spectra of two possible X-ray counterparts of 1FGL J1311.7−3429 in the photon energy range 0.4–8.0 keV fitted with the best-fit power-law model. FI data are represented in black, and BI data are in gray.

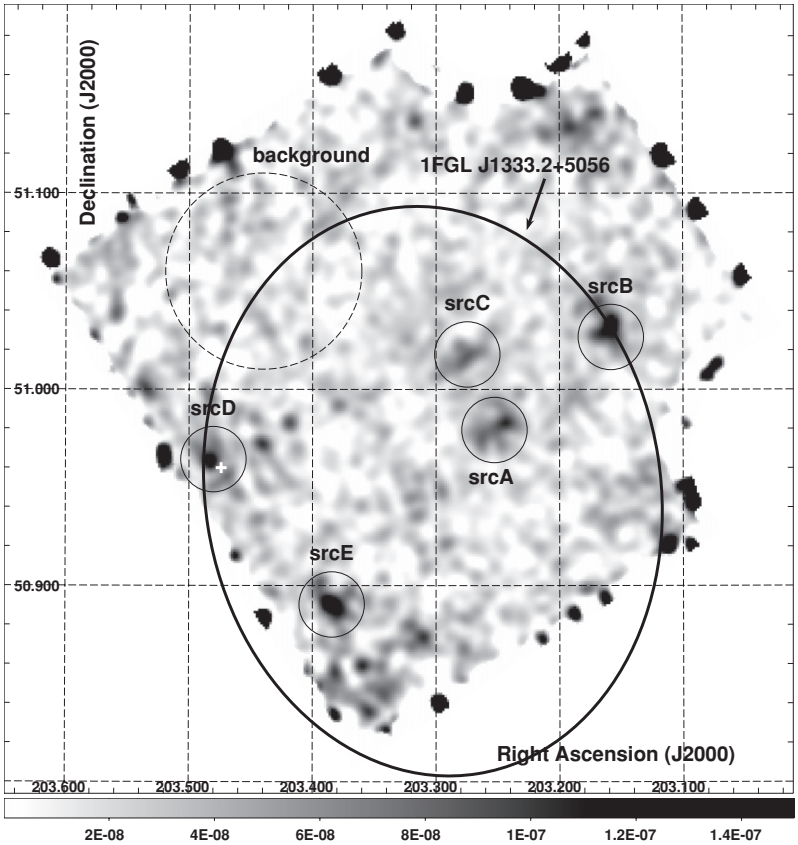

Figure 7. *Suzaku*/XIS FI (XIS0+3) image of the 1FGL J1333.2+5056 region in the 0.4–10 keV photon energy range. The image shows the relative excess of smoothed photon counts (arbitrary units indicated in the bottom bar) and is displayed with linear scaling. The regions enclosed by the solid and dashed circles are the source and background regions, respectively. The thick solid ellipse denotes the 95% position error of 1FGL J1333.2+5056. Within this error circle, several potential X-ray counterparts of the γ-ray object were found. The white cross marks the position of the active galaxy CLASS J1333+5057.

further analysis, we set the extraction region to encircle this bright source with a radius of 3′. The corresponding light curve of the newly discovered X-ray source is shown in Figure 11 with 620 s binning. The light curve is consistent (at the level of >99%) with a constant X-ray flux within the errors (χ^2/dof = 26.4/56) and average count rate of 4.07×10^{-2} counts s^{-1}. Figure 12 shows the X-ray spectrum of the analyzed source. A power-law model (photon index $\Gamma \simeq 1.6$) with Galactic absorption provided the best fit to the data, and the obtained best-fit parameters are given in Table 9.

The X-ray point source found at the edge of the 1FGL error circle is positionally coincident (offset by 15″, which is much less the *Suzaku*/XIS position accuracy of ∼1′) with the $z = 1.743$ FSRQ CLASS J2017+0603 (Myers et al.

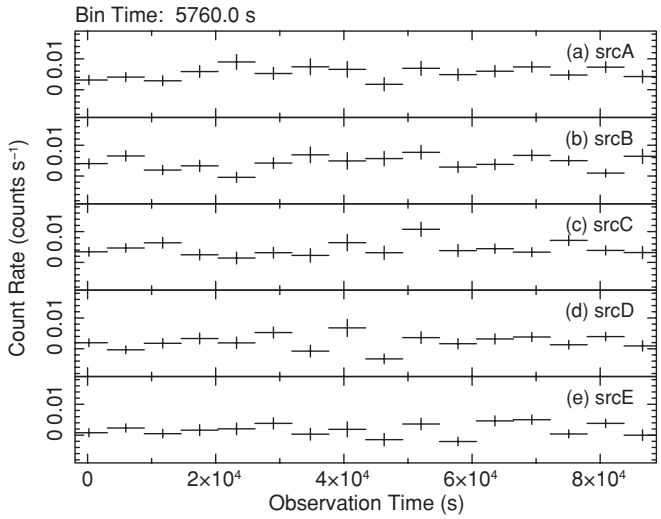

Figure 8. *Suzaku*/XIS light curves of potential X-ray counterparts of 1FGL J1333.2+5056 with the applied time binning of 5760 s. The zero point of time is MJD 54983.4274 (TDB).

Table 7
Count Rates and Constant Flux Fits for X-ray Sources within the Error Circle of 1FGL J1333.2+5056

Source	Average Count Rate and Error (10^{-3} counts s^{-1})	χ^2/dof	Prob. (%)
src A	5.47 ± 0.51	14.9/15	46.08
src B	4.40 ± 0.49	22.4/15	9.73
src C	4.37 ± 0.48	18.8/15	22.28
src D	2.19 ± 0.44	20.5/15	15.25
src E	1.70 ± 0.44	23.3/15	7.86

2003). This blazar has been listed in the first *Fermi*/LAT AGN Catalog (Abdo et al. 2010d) as being possibly associated with 1FGL J2017.3+0603, even though the probability for such an association was not quantified. We denote its position in Figure 10 with a white cross. More recently, radio and γ-ray pulsations with pulse periods of 2.9 ms have been discovered using the Nancay radio telescope well within the *Fermi*/LAT error circle of 1FGL J2017.3+0603 (Cognard et al. 2011), pointing instead to a pulsar (rather than blazar) association of this source. In Figure 10, we mark the position of the MSP PSR J2017+0603 with a black cross. As shown, no X-ray counterpart of the pulsar has been detected by *Suzaku*/XIS. In order to determine the corresponding X-ray flux upper limit, we set an additional source region within a 1′ radius around the position of the radio pulsar and assumed a power-law emission spectrum with photon index $\Gamma = 2$. The resulting 90% confidence X-ray upper limit is $S_{2-8\,\mathrm{keV}} < 2.61 \times 10^{-14}$ erg cm^{-2} s^{-1}.

Table 9
Fitting Parameters for 1FGL J2017.3+0603 for the Power-law Model

Parameter	Value and Error
N_{H} (10^{22} cm^{-2})	0.1309 (fixed)
Γ	$1.59^{+0.15}_{-0.15}$
Norm.	$(5.03^{+0.68}_{-0.66}) \times 10^{-5}$
χ^2	34.8
dof	38
Reduced χ^2	0.916
Flux (2–8 keV) (erg cm^{-2} s^{-1})	$(1.99^{+0.28}_{-0.27}) \times 10^{-13}$

4. DISCUSSION

4.1. The Observed Sample

Within the error circle of the unidentified γ-ray object 1FGL J1231.4−1410, only one X-ray source was found, which is positionally consistent with the radio/γ-ray MSP PSR J1231−1411 (Ransom et al. 2010; see Figure 1). The broadband spectrum of 1FGL J1231.1−1410/PSR J1231−1411, including our *Suzaku*/XIS data and the derived UVOT optical/UV upper limits from *Swift*, is shown in Figure 13. We note that the SED is reminiscent of that of the Geminga pulsar (Thompson et al. 1999) or 3EG J1835+5918 (Halpern et al. 2002). Hence, a consistent picture emerges in which the $kT \simeq 0.16$ keV blackbody component of the newly discovered X-ray counterpart of 1FGL J1231.1−1410 originates as a thermal emission from the surface of a rotating magnetized neutron star, a pulsar, while the γ-ray emission detected by *Fermi*/LAT may be accounted for by the emission of ultra-relativistic electrons present within the pulsar magnetosphere. The non-thermal X-ray component is then likely to be produced within the magnetosphere of PSR J1231−1411 as well, even though one may also expect some contribution from the outer regions (pulsar wind nebulae) to the detected hard X-ray continuum.

Assuming that PSR J1231−1411 is a typical MSP with spin period $P = 3.68$ ms and a spin-down rate $\dot{P} = 2.1 \times 10^{-20}$ s s^{-1} (see Ransom et al. 2010), one can calculate the corresponding spin-down luminosity as $L_{\mathrm{sd}} = 4\pi^2 I \dot{P} P^{-3} \simeq 2 \times 10^{34}$ erg s^{-1} and the magnetic field intensity at the light cylinder (radius, $R = cP/2\pi$) as $B_{\mathrm{lc}} \simeq 4\pi^2 (3 I \dot{P}/2c^3 P^5)^{1/2} \simeq 5 \times 10^4$ G, where $I = 10^{45}$ g cm^2 is the star's moment of inertia. Meanwhile, for the claimed distance $d \simeq 0.4$ kpc (Ransom et al. 2010),

Table 8
Fitting Parameters for 1FGL J1333.2+5056 for the Power-law Model

Parameter	src A Value and Error	src B Value and Error	src C Value and Error	src D Value and Error	src E Value and Error
N_{H} (10^{20} cm^{-2})	1.09 (fixed)	1.09 (fixed)	1.09 (fixed)	1.09 (fixed)	1.09 (fixed)
Γ	$2.35^{+0.35}_{-0.32}$	$1.48^{+0.29}_{-0.27}$	$1.51^{+0.31}_{-0.29}$	$1.76^{+0.60}_{-0.52}$	$2.50^{+0.69}_{-0.58}$
Norm. ($\times 10^{-5}$)	$1.57^{+0.28}_{-0.28}$	$1.07^{+0.27}_{-0.26}$	$0.84^{+0.22}_{-0.22}$	$0.77^{+0.31}_{-0.30}$	$1.34^{+0.36}_{-0.37}$
χ^2	13.0	7.33	18.3	12.7	11.4
dof	18	18	18	16	12
Reduced χ^2	0.720	0.407	1.02	0.796	0.949
Flux (2–8 keV) ($\times 10^{-14}$ erg cm^{-2} s^{-1})	$2.16^{+0.88}_{-0.75}$	$4.98^{+1.46}_{-1.37}$	$3.77^{+1.17}_{-1.11}$	$2.41^{+1.55}_{-1.26}$	$1.52^{+1.41}_{-0.94}$

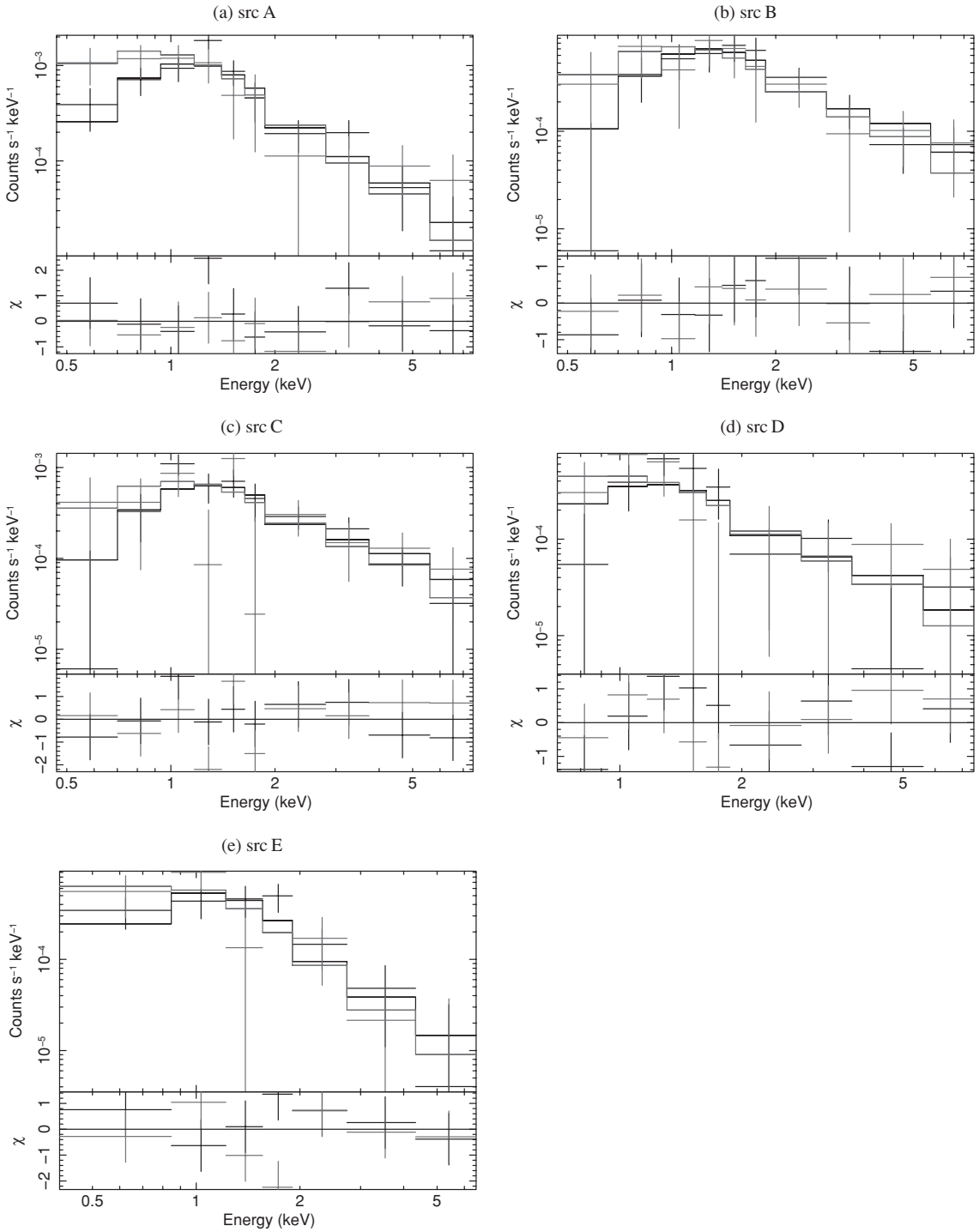

Figure 9. *Suzaku*/XIS spectra of the selected possible X-ray counterparts of 1FGL J1333.2+5056 fitted with a power-law model. FI data are represented in black, and BI data are in gray.

the observed γ-ray luminosity of PSR J1231−1411 leads as $L_\gamma \simeq 2 \times 10^{33}$ erg s^{-1}, its non-thermal X-ray luminosity is $L_{\rm X} \simeq 10^{30}$ erg s^{-1}, and the total X-ray luminosity is $L_{\rm X/tot} \sim 3 \times 10^{30}$ erg s^{-1}. These values are then consistent with the MSP scenario—outer-magnetosphere models in particular—in a framework of which one should expect $L_\gamma \sim 0.1\, L_{\rm sd}$ (Abdo et al. 2009d) and $L_{\rm X} \sim 10^{-3}\, L_{\rm sd}$ (Becker & Truemper 1997; Gaensler & Slane 2006; Zhang et al. 2007), with relatively large dispersion, however. Interestingly, the synchrotron X-ray luminosity produced close to the light cylinder within the expected magnetic field $B_{\rm lc}$ and a fraction (say 10%) of the volume $V \sim R^3$ would then be close to the observed non-thermal X-ray luminosity assuming rough energy equipartition between ultra-relativistic electrons and the magnetic field.

In the case of 1FGL J1311.7−3429, two potential X-ray counterparts have been discovered in our *Suzaku* observations. The association of this *Fermi* object with the northern source src A is more likely, since the southern X-ray spot src B is located only marginally within the 95% *Fermi*/LAT error circle of the γ-ray emitter. Yet the classification of 1FGL J1311.7−3429/src A,

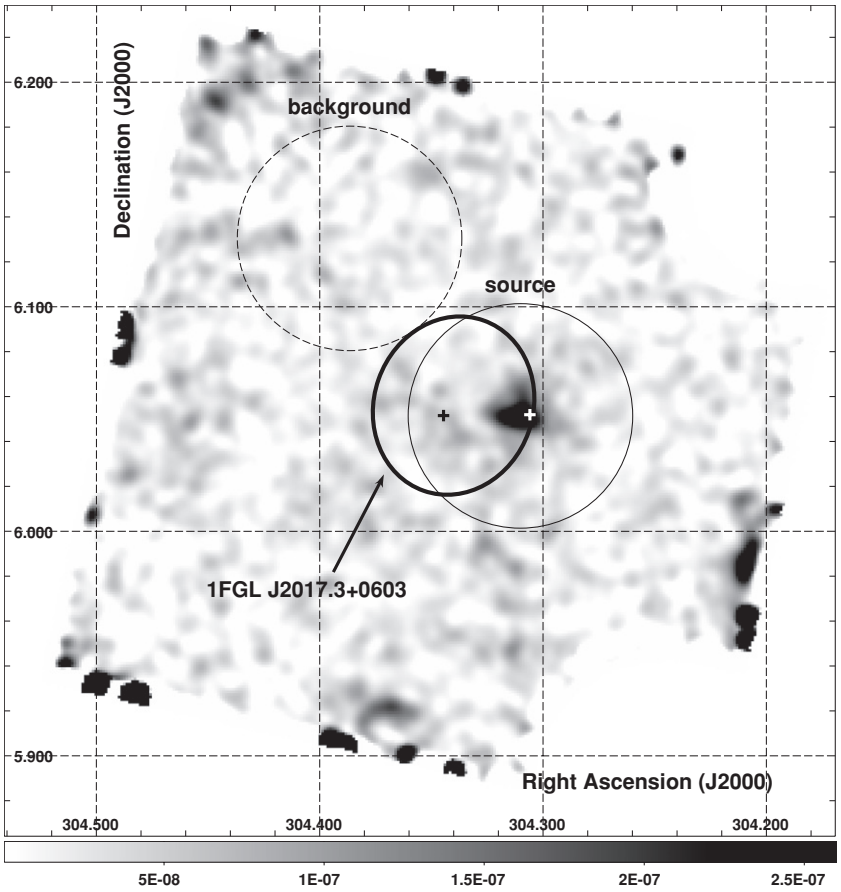

Figure 10. *Suzaku*/XIS FI (XIS0+3) image of the 1FGL J2017.3+0603 region in the 0.4–10 keV photon energy range. The image shows the relative excess of smoothed photon counts (arbitrary units indicated in the bottom bar) and is displayed with linear scaling. The regions enclosed by the solid and dashed circles are the source and background regions, respectively. The thick solid circle denotes the 95% position error of 1FGL J2017.3+0603. One X-ray point source was found within this error circle. The white cross denotes the position of the blazar CLASS J2017+0603. The black cross denotes the position of the radio MSP, PSR J2017+0603 (Cognard et al. 2011).

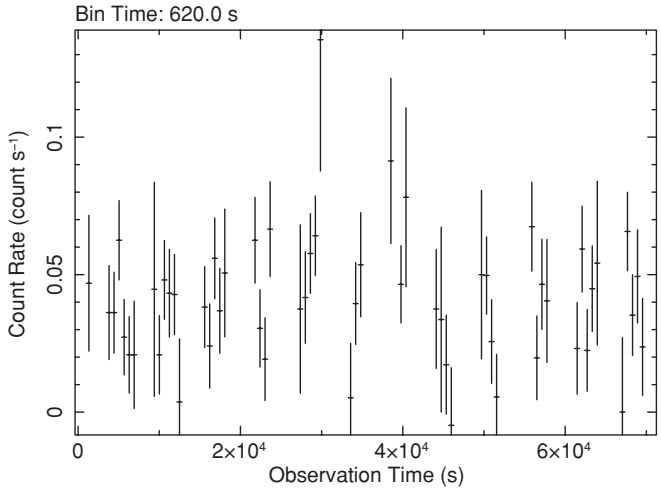

Figure 11. *Suzaku*/XIS light curve of an X-ray point source within the error circle of 1FGL J2017.3+0603 with the applied 620 s time binning. The zero point of time is MJD 55131.4285 (TDB).

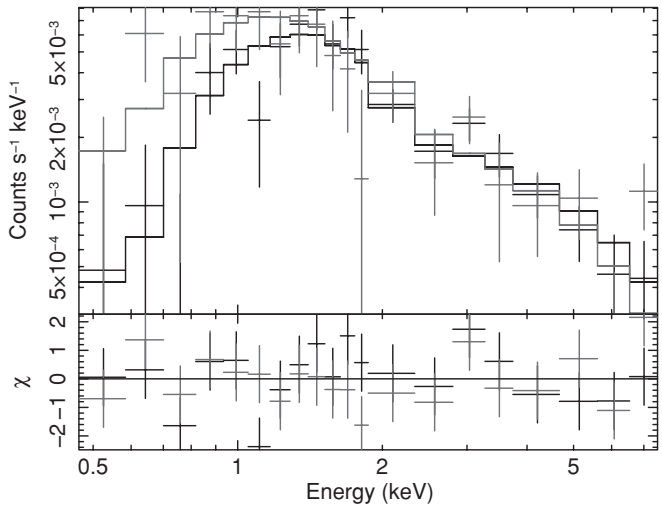

Figure 12. *Suzaku*/XIS spectrum of the potential X-ray counterpart of 1FGL J2017.3+0603 with the best-fit power-law model. FI data are shown in black, and BI data are in gray.

for which the broadband spectrum (including radio and optical upper limits) is shown in Figure 14, remains vague. Currently, no radio or γ-ray pulsations have been found at the position of 1FGL J1311.7−3429, and this favors an extragalactic origin of the detected high-energy emission. And indeed, the flat X-ray continuum ($\Gamma \simeq 1.4$) and the γ-ray–to–X-ray energy flux ratio $\gtrsim$100 (with $S_{0.1-10\,\mathrm{GeV}} \simeq 6.4 \times 10^{-11}$ erg cm^{-2} s^{-1} as given in the 1FGL catalog) would be consistent with the characteristics of luminous blazars of the FSRQ type (e.g., Sikora et al. 2009). On the other hand, however, the radio upper limit indicating that the GHz energy flux is $\simeq 10^{-5}$ times smaller than the GeV energy

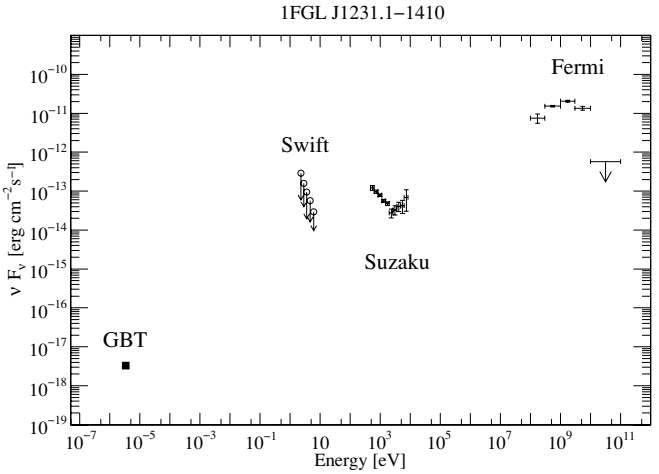

Figure 13. Broadband spectrum of 1FGL J1231.1−1410/PSR J1231−1411. The X-ray data points represent the weighted mean of *Suzaku*/XIS FI and BI data. The γ-ray data points are taken from the 1FGL catalog (Abdo et al. 2010c). The radio data point is derived from the MSP PSR J1231−1411 observed with the Green Bank Telescope by Ransom et al. (2010). The optical/UV upper limits were derived from the *Swift*/UVOT observation.

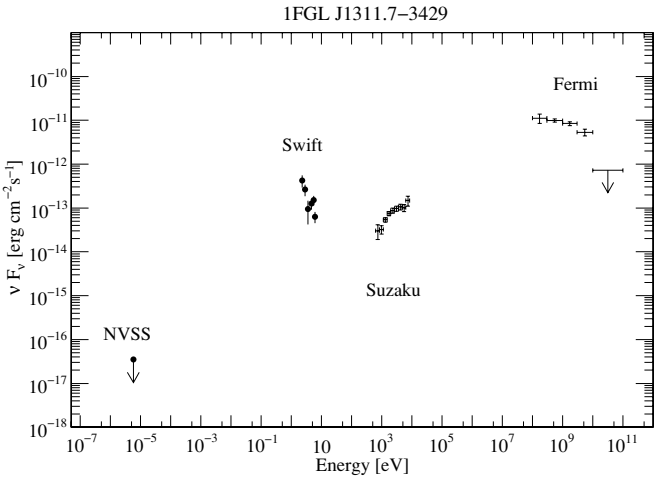

Figure 14. Broadband spectrum of 1FGL J1311.7−3429. The X-ray data points represent the weighted mean of *Suzaku*/XIS FI and BI data for src A. The γ-ray data points are taken from the 1FGL catalog (Abdo et al. 2010c). The radio upper limit is taken from the NVSS catalog (Condon et al. 1998). The optical/UV data points show the *Swift*/UVOT data.

flux invalidates the blazar nature of 1FGL J1311.7−3429. That is because all active galaxies established until now as γ-ray emitters are characterized by relatively strong, Doppler-boosted radio emission. In particular, radio energy fluxes of bona fide blazars included in 0FGL are, for a given *Fermi*/LAT photon flux of $\sim 10^{-7}$ photons cm^{-2} s^{-1}, at least an order of magnitude higher than the energy flux implied by the NVSS upper limits for src A (see, e.g., Kovalev et al. 2009). In addition, a very prominent 10 ks-long X-ray flare detected from src A, together with the steady GeV flux of 1FGL J1311.7−3429, would not easily match a typical behavior of FSRQs: this class of blazars is known for displaying dramatic variability at GeV photon energies, but only modest variations in the X-ray band. Therefore, the nature of the analyzed *Fermi* source and its newly discovered *Suzaku* counterpart remains an open question.

Within the error circle of 1FGL J1333.2+5056, our *Suzaku*/XIS observations revealed the presence of several weak X-ray flux maxima with possibly diverse spectral properties

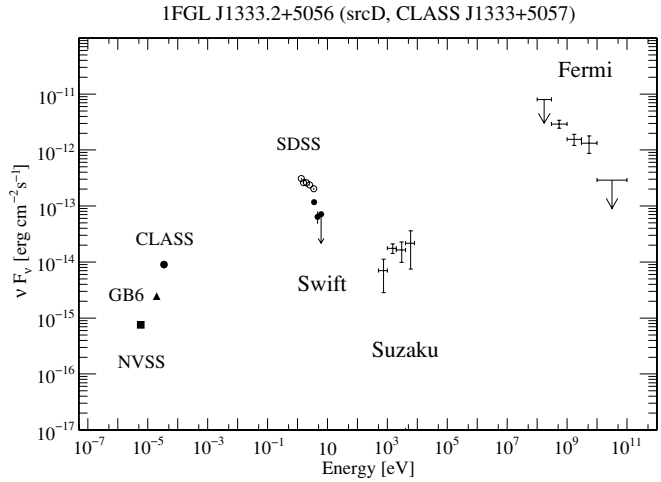

Figure 15. Broadband spectrum of 1FGL J1333.2+5056/CLASS J1333+5057. The X-ray data points represent the weighted mean of *Suzaku*/XIS FI and BI data for src D which coincides with the CLASS source. The γ-ray data points are taken from the 1FGL catalog (Abdo et al. 2010c). The radio data points, representing blazar CLASS J1333+5057, are taken from the CLASS catalog (filled circle; Myers et al. 2003), NVSS catalog (filled square; Condon et al. 1998), and GB6 catalog (filled triangle; Gregory et al. 1996). Optical data points (open circle) were derived from SDSS J133353.78+505735.9 (SDSS Data Release 6; Adelman-McCarthy et al. 2008), optical/UV data points and upper limits (filled circle) are the *Swift*/UVOT data.

(as indicated by the spectral analysis hampered by the limited photon statistics). One of the detected X-ray sources (src D) coincides with the high-redshift blazar CLASS J1333+5056 ($z = 1.362$). The broadband SED of 1FGL J1333.2+5056/CLASS J1333+5056/src D is presented in Figure 15, including the LAT γ-ray, *Suzaku* X-ray, archival radio, and newly analyzed *Swift*/UVOT data for the blazar. The constructed SED reveals two distinct radiative components, consisting of a low-energy synchrotron bump and an (energetically dominant) high-energy inverse-Compton continuum, reminiscent of typical broadband spectra for blazars of the FSRQ type (Ghisellini et al. 1998). Note that the X-ray-to-γ-ray flux ratio of $\simeq 10^3$ implied by Figure 15, as well as the relatively large radio flux, would be both in agreement with the blazar identification of 1FGL J1333.2+5056. In addition, we note that the discussed *Fermi* object is the most variable in γ-rays out of all four *Fermi* targets studied in this paper, with the variability index of 38 (which indicates a $<1\%$ probability of a steady flux; see Abdo et al. 2010c). The additional support for the blazar association is offered by the fact that the γ-ray continuum of 1FGL J1333.2+5056 is the steepest among the four *Fermi* objects we observed, with the photon index $\simeq 2.5 \pm 0.1$, which is compatible with the mean γ-ray photon index of the FSRQ population reported in the 1FGL, namely 2.47 ± 0.19 (Abdo et al. 2010f).

Finally, in the case of 1FGL J2017.3+0603, the MSP PSR J2017+0603 was newly discovered by the Nancay Radio Telescope (Cognard et al. 2011), and the association between the radio and γ-ray sources was confirmed by the pulse detection with the same period in the LAT data. Interestingly, in our *Suzaku*/XIS exposure we have only detected the high-redshift blazar ($z = 1.743$) CLASS J2017+0603, but not the pulsar. The same is true for the *Swift*/UVOT observation (Cognard et al. 2011), which resulted in analogous flux and upper limit measurements in the optical for the blazar and pulsar, respectively. The constructed radio to X-ray SEDs for the pulsar and blazar systems are shown in Figure 16 together with the LAT spectrum. Regarding the pulsar, Cognard et al.

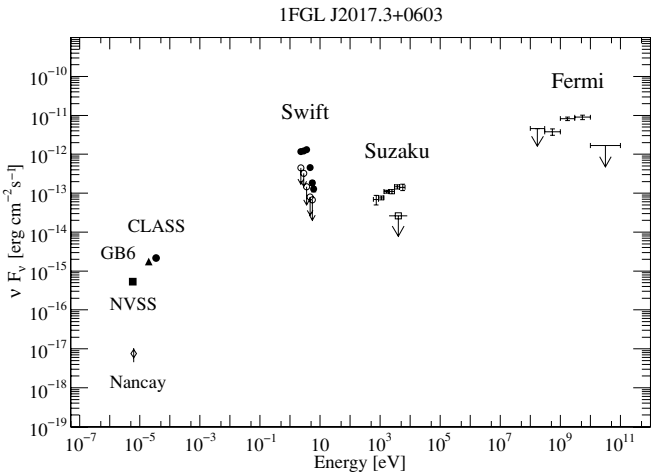

Figure 16. Broadband spectrum of 1FGL J2017.3+0603. The X-ray data points represent the weighted mean of *Suzaku*/XIS FI and BI data for active galaxy CLASS J2017+0603. The X-ray upper limit (open square) is derived from the location of the MSP PSR J2017+0603. The γ-ray data points are taken from the 1FGL catalog (Abdo et al. 2010c). The radio data points, representing CLASS J2017+0603, are taken from the CLASS catalog (filled circle; Myers et al. 2003), NVSS catalog (filled square; Condon et al. 1998), and GB6 catalog (filled triangle; Gregory et al. 1996). The open diamond shaped point in radio shows the MSP PSR J2017+0603 observed with the Nancay Radio Telescope (Cognard et al. 2011) and also the optical/UV upper limits (open circle) show the MSP observed with *Swift*/UVOT (Cognard et al. 2011). The optical/UV data points (corresponding filled circle) show the blazar CLASS J2017+0603 observed with *Swift*/UVOT.

(2011) discovered that PSR J2017+0603 is located at a distance $d \simeq 1.6$ kpc and as such is characterized by the spin-down luminosity $L_{\rm sd} \sim 1.34 \times 10^{34}$ erg s^{-1}. The X-ray (2–8 keV) luminosity derived from the *Suzaku*/XIS upper limit for this pulsar, $L_{\rm X} < 8.0 \times 10^{30}$ erg s^{-1}, is then consistent with the expected "pulsar-like" luminosity ratio $L_{\rm X}/L_{\rm sd} \sim 10^{-3}$. The overall curved γ-ray spectrum of 1FGL J2017.3+0603, characterized by the small photon index $\simeq 1.88 \pm 0.05$, supports the pulsar association. On the other hand, the relatively large radio flux of CLASS J2017+0603, together with the X-ray-to-γ-ray flux ratio $\simeq 300$ for the 1FGL J2017.3+0603/CLASS J2017+0603 system, is in some level of agreement with the blazar interpretation. The γ-ray photon index of 1FGL J2017.3+0603 is however rather flat for an FSRQ and represents a $\sim 3\sigma$ deviation from the distribution observed for FSRQs (mean = 2.47, $\sigma = 0.19$; see Abdo et al. 2010f), thus making the association with the FSRQ less likely. Although the detected pulsations in radio and γ-rays are key to the identification of the γ-ray source with a pulsar, there may be some contaminating flux from the blazar. Indeed, the chance probability of finding a CLASS-like background blazar in the *Fermi* error circle of this source is $\sim$0.003%. Considering that there are over 1400 sources in the 1FGL catalog, such "mixed" cases could be expected.

4.2. Implications

What class of astrophysical objects can be in general associated with the unidentified high Galactic latitude γ-ray sources? It was noted, for example, that compact and relatively nearby molecular clouds exist at $|b| > 10^\circ$, and these should emit γ-rays at least at some level. Torres et al. (2005) argued, however, that the expected GeV emission of such clouds is too low to account for the observed fluxes of unidentified EGRET sources, and the same applies to the bright unidentified *Fermi*/LAT objects. Other classes of possible counterparts proposed were radio-quiet pulsars and isolated neutron stars (e.g., Yadigaroglu & Romani 1995), and this idea has indeed been validated by the subsequent multi-frequency studies, as discussed in Section 1. We note in this context that the Galactic origin of high-latitude γ-ray emitters is especially probable for the objects located at $10^\circ \leqslant |b| \leqslant 30^\circ$ within the Gould Belt ($\sim$0.3 kpc from the Earth), which constitutes an aggregation of massive late-type stars, molecular clouds, and supernova remnants (Grenier 2000).

A probably more challenging population of γ-ray emitters is represented by the isotropic component of the unidentified EGRET objects, consisting of about 60 sources (about one-third of which with the Galactic latitudes $|b| > 45^\circ$, including several non/weakly variable during the EGRET observations; Özel & Thompson 1996; Gehrels et al. 2000). For those sources, Totani & Kitayama (2000) have, for example, suggested associations with large-scale shocks produced during the structure formation in the intergalactic medium (see also Waxman & Loeb 2000). Totani & Kitayama explored the connection between steady GeV objects located off the Galactic plane and labeled in the 3EG catalog as "possibly extended," with dynamically forming clusters of galaxies (and not single virialized cluster systems; see Kawasaki & Totani 2002). However, the non-variable nature of the γ-ray emission of several of the considered objects was questioned (see Reimer et al. 2003 and references therein), and the high efficiency of the particle acceleration at the structure formation shocks required by the model was also noted (e.g., Keshet et al. 2003).

Radio galaxies are prime candidates for the unidentified high Galactic latitude EGRET sources, especially since the only confirmed non-blazar AGN detected previously at GeV photon energies was the nearby radio galaxy Centaurus A (Steinle et al. 1998; Sreekumar et al. 1999). However, no other radio galaxy has been firmly detected by EGRET at the significance level high enough ($\geqslant 4\sigma$) to be included in the 3EG (Hartman et al. 1999). Moreover, Cillis et al. (2004), who applied a stacking analysis of the EGRET data for a sample of the brightest and/or the closest radio and Seyfert galaxies, showed that "no detection significance greater than 2σ has been found for any subclass, sorting parameter, or number of objects co-added." Nevertheless, Mukherjee et al. (2002) argued that the most likely counterpart to the unidentified EGRET source 3EG J1621+8203 is the bright radio galaxy NGC 6251. A marginal detection of 3C111 with EGRET has also been reported (Hartman et al. 2008). We also note that Combi et al. (2003) reported the discovery of a new radio galaxy within the location error circle of the unidentified γ-ray source 3EG J1735−1500. The identification of 3EG J1735−1500 was however controversial due to the presence of another likely (blazar-type) candidate within the EGRET error contours (Sowards-Emmerd et al. 2004). The most recent analysis based on the 15 months of *Fermi*/LAT data resulted in the detection of 11 non-blazar-type AGNs (all radio galaxies), including the aforementioned cases of NGC 6251 and 3C111 (Abdo et al. 2010g). The idea that some fraction of unidentified γ-ray emitters may be associated with faint radio galaxies is therefore validated, although this should rather apply to only dimmer *Fermi* objects and not to the population of exceptionally bright γ-ray sources detected already by EGRET.

The *Suzaku*/XIS studies of four bright *Fermi*/LAT objects reported here provide an important contribution to the debate regarding the nature of unidentified γ-ray emitters located at high Galactic latitudes. In particular, our observations support

the idea that a significant fraction of such objects may be associated with old ($\gtrsim$ Gyr) MSPs present within the Galactic halo and Earth's neighborhood (such as 1FGL J1231.1−1410 and 1FGL J2017.3+0603). Yet not all of the unidentified *Fermi* objects are related to the pulsar phenomenon. Instead, some of those may be hosted by active galaxies, most likely by the luminous and high-redshift blazars of the FSRQ type (1FGL J1333.2+5056 is a good blazar candidate, for example). However, there still remain unidentified sources (e.g., 1FGL J1311.7−3429), for which neither blazar nor pulsar scenarios seem to apply. For these, ultra-deep multi-wavelength studies are probably needed to unravel their physical nature.

5. SUMMARY

In this paper, we reported on the results of deep X-ray follow-up observations of four unidentified γ-ray sources detected by the *Fermi*/LAT instrument at high Galactic latitudes ($|b| > 10^{\circ}$) using the XIS on board the *Suzaku* satellite. All of the studied objects have been detected at high significance ($>10\sigma$) during the first three months of the *Fermi*/LAT operation. For some of them, possible associations with pulsars and blazars have been recently discussed, and our observations provide an important contribution to this debate. In particular, an X-ray point source was newly found within 95% error circle of 1FGL J1231.1−1410. The X-ray spectrum of the discovered *Suzaku* counterpart of 1FGL J1231.1−1410 is well fitted by a blackbody emission with a temperature of $kT \simeq 0.16$ keV plus an additional power-law component with a differential photon index $\Gamma \simeq 1.8$. This supports the recently claimed identification of this source with an MSP, PSR J1231−1411. For the remaining three *Fermi* objects, the performed X-ray observations are less conclusive. In the case of 1FGL J1311.7−3429, two possibly associated X-ray point sources were newly found. Even though the 0.4–10 keV spectral and variability properties for those could be robustly accessed, the physical nature of the X-ray emitters and their relations with the γ-ray source remain unidentified. Similarly, we found several weak X-ray sources in the field of 1FGL J1333.2+5056, one coinciding with the high-redshift blazar CLASS J1333+5057. We argue that the available data are consistent with the physical association between these two objects, even though we were not able to identify robustly the *Suzaku* counterpart of the γ-ray emitter due to the large positional uncertainty of 1FGL J1333.2+5056. Finally, we found an X-ray point source in the vicinity of 1FGL J2017.3+0603. This *Fermi* object was recently suggested to be associated with a newly discovered MSP, PSR J2017+0603, because of the detection of radio and γ-ray pulsations. However, we did not detect the X-ray counterpart of the pulsar, but instead of the high-redshift blazar CLASS J2017+0603 located within the error circle of 1FGL J2017.3+0603. Still, the resulting upper limits for the X-ray emission do not invalidate the pulsar association.

Ł.S. is grateful for the support from Polish MNiSW through grant N-N203-380336.

REFERENCES

Abdo, A. A., et al. (*Fermi*-LAT Collaboration) 2009a, ApJ, 700, 597
Abdo, A. A., et al. (*Fermi*-LAT Collaboration) 2009b, ApJ, 700, 1059
Abdo, A. A., et al. (*Fermi*-LAT Collaboration) 2009c, ApJS, 183, 46
Abdo, A. A., et al. (*Fermi*-LAT Collaboration) 2009d, Science, 325, 840
Abdo, A. A., et al. (*Fermi*-LAT Collaboration) 2010a, ApJ, 712, 1209
Abdo, A. A., et al. (*Fermi*-LAT Collaboration) 2010b, ApJ, 712, 957
Abdo, A. A., et al. (*Fermi*-LAT Collaboration) 2010c, ApJS, 188, 405
Abdo, A. A., et al. (*Fermi*-LAT Collaboration) 2010d, ApJ, 715, 429
Abdo, A. A., et al. (*Fermi*-LAT Collaboration) 2010e, ApJS, 187, 460
Abdo, A. A., et al. (*Fermi*-LAT Collaboration) 2010f, ApJ, 720, 435
Abdo, A. A., et al. (*Fermi*-LAT Collaboration) 2010g, ApJ, 720, 912
Adelman-McCarthy, J. K., et al. 2008, ApJS, 175, 297
Atwood, W. B., et al. 2009, ApJ, 697, 1071
Becker, W., & Truemper, J. 1997, A&A, 326, 682
Casandjian, J.-M., & Grenier, I. A. 2008, A&A, 489, 849
Cillis, A. N., Hartman, R. C., & Bertsch, D. L. 2004, ApJ, 601, 142
Cognard, I., et al. 2011, ApJ, submitted
Combi, J. A., Romero, G. E., Paredes, J. M., Torres, D. F., & Ribo, M. 2003, ApJ, 588, 731
Condon, J. J., Cotton, W. D., Greisen, E. W., Yin, Q. F., Perley, R. A., Taylor, G. B., & Broderick, J. J. 1998, AJ, 115, 1693
Day, C., et al. 1998, The ASCA Data Reduction Guide, Tech. Rep. (Greenbelt: NASA GSFC), v.2.0
Dickey, J. M., & Lockman, F. J. 1990, ARA&A, 28, 215
Gaensler, B. M., & Slane, P. O. 2006, ARA&A, 44, 17
Gehrels, N., & Michelson, P. 1999, Astropart. Phys., 11, 277
Gehrels, N., et al. 2000, Nature, 404, 363
Ghisellini, G., Celotti, A., Fossati, G., Maraschi, L., & Comastri, A. 1998, MNRAS, 301, 451
Gregory, P. C., Scott, W. K., Douglas, K., & Condon, J. J. 1996, ApJS, 103, 427
Grenier, I. A. 2000, A&A, 364, 93
Halpern, J. P., Eracleous, M., Mukherjee, R., & Gotthelf, E. V. 2001, ApJ, 551, 1016
Halpern, J. P., Gotthelf, E. V., Mirabal, N., & Camilo, F. 2002, ApJ, 573, L41
Halpern, J. P., et al. 2008, ApJ, 688, L33
Hartman, R. C., Kadler, M., & Tueller, J. 2008, ApJ, 688, 852
Hartman, R. C., et al. 1999, ApJS, 123, 79
Ishisaki, Y., et al. 2007, PASJ, 59, 113
Kawasaki, W., & Totani, T. 2002, ApJ, 576, 679
Keshet, U., Waxman, E., Loeb, A., Springel, V., & Hernquist, L. 2003, ApJ, 585, 128
Kokubun, M., et al. 2007, PASJ, 59, 53
Kovalev, Y. Y., et al. 2009, ApJ, 696, 17
Koyama, K., et al. 2007, PASJ, 59, 23
Mirabal, N., Halpern, J. P., Eracleous, M., & Becker, R. H. 2000, ApJ, 541, 180
Mitsuda, K., et al. 2007, PASJ, 59, 1
Morrison, R., & McCammon, D. 1983, ApJ, 270, 119
Mukherjee, R., Gotthelf, E. V., Halpern, J. P., & Tavani, M. 2000, ApJ, 542, 740
Mukherjee, R., & Halpern, J. 2004, in Cosmic Gamma-Ray Sources, Vol. 304, ed. K. S. Cheng & G. E. Romero (Dordrecht: Kluwer), 311
Mukherjee, R., Halpern, J., Mirabal, N., & Gotthelf, E. V. 2002, ApJ, 574, 693
Myers, S. T., et al. 2003, MNRAS, 341, 1
Nolan, P. L., Tompkins, W. F., Grenier, I. A., & Michelson, P. F. 2003, ApJ, 597, 615
Özel, M. E., & Thompson, D. J. 1996, ApJ, 463, 105
Ransom, S. M., et al. 2010, ApJ, 727, L16
Reimer, O. 2001, in Proc. The Nature of Unidentified Galactic High-Energy Gamma-Ray Sources, Vol. 267, ed. A. Carraminana, O. Reimer, & D. J. Thompson (Dordrecht: Kluwer), 17
Reimer, O., Pohl, M., Sreekumar, P., & Mattox, J. R. 2003, ApJ, 588, 155
Reimer, O., et al. 2001, MNRAS, 324, 772
Shaw, M. S., Romani, R. W., Healey, S. E., Cotter, G., Michelson, P. F., & Readhead, A. C. S. 2009, ApJ, 704, 477
Sikora, M., Stawarz, Ł., Moderski, R., Nalewajko, K., & Madejski, G. M. 2009, ApJ, 704, 38
Sowards-Emmerd, D., Romani, R. W., & Michelson, P. F. 2003, ApJ, 590, 109
Sowards-Emmerd, D., Romani, R. W., & Michelson, P. F. 2004, ApJ, 609, 564
Sreekumar, P., Bertsch, D. L., Hartman, R. C., Nolan, P. L., & Thompson, D. J. 1999, Astropart. Phys., 11, 221
Steinle, H., et al. 1998, A&A, 330, 97
Takahashi, T., et al. 2007, PASJ, 59, 35
Tavani, M., et al. 2009, A&A, 502, 995
Tawa, N., et al. 2008, PASJ, 60, 11
Thompson, D. J., et al. 1999, ApJ, 516, 297
Torres, D. F., Dame, T. M., & Digel, S. W. 2005, ApJ, 621, L29
Totani, T., & Kitayama, T. 2000, ApJ, 545, 572
Waxman, E., & Loeb, E. 2000, ApJ, 545, L11
Yadigaroglu, I. A., & Romani, R. W. 1995, ApJ, 449, 211
Zhang, L., Fang, J., & Chen, S. B. 2007, ApJ, 666, 1165